Mechanisms of the Effect of Dopants and $P(O_2)$ on the Improper Ferroelastic Phase Transition in $SrTiO_3$

Alexander Tkach,[†] Paula M. Vilarinho,*[,†] Andrei L. Kholkin,[†] Ian M. Reaney,[‡] Jan Pokorny,[§] and Jan Petzelt[§]

Department of Ceramics and Glass Engineering, CICECO, University of Aveiro, 3810-193 Aveiro, Portugal, Department of Engineering Materials, University of Sheffield, Sheffield S1 3JD, United Kingdom, and Department of Dielectrics, Institute of Physics, Czech Academy of Sciences, Na Slovance 2, 18040 Prague 8, Czech Republic

Received July 8, 2007. Revised Manuscript Received September 17, 2007

Perovskite-structured $SrTiO_3$ undergoes a cubic (*Pm*3*m*) to tetragonal (*I*4/*mcm*) transition at ~108 K (T_a) associated with rotations of the O octahedra in the antiphase around the [001] direction. This phase transition gives rise to modes at the R point of the Brillouin zone in the Raman spectra and superlattice reflections at $^1/_2${odd–odd–odd}. The effect on T_a of La^{3+} and Mn^{2+} A-site substitution and Mn^{4+} and Mg^{2+} B-site substitution in polycrystalline $SrTiO_3$ processed in air and sintering $SrTi_{0.95}Mn_{0.05}O_{3-\delta}$ in different $P(O_2)$ has been studied using in situ Raman spectroscopy and electron diffraction. The transition temperature was raised when Mn^{2+} and La^{3+} were substituted for Sr^{2+} but lowered for Mn^{4+} and Mg^{2+} substitution on the Ti site. Sintering $SrTi_{0.95}Mn_{0.05}O_{3-\delta}$ in N_2 reduced T_a, but sintering in O_2 had a negligible effect compared to air. It is proposed that two mechanisms are responsible for the modification of T_a: (i) the creation of oxygen vacancies by acceptor doping (Mg^{2+} ions on the Ti site) and sintering $SrTi_{0.95}Mn_{0.05}O_{3-\delta}$ in low $P(O_2)$ and (ii) adjustment of the perovskite tolerance factor (*t*) when, e.g., La^{3+} (1.36 Å) and Mn^{2+} (1.27 Å) substitute for Sr^{2+} (1.44 Å, decrease in *t*) and Mn^{4+} (0.53 Å) substitutes for Ti^{4+} (0.605 Å, increase in *t*).

Introduction

The undistorted cubic perovskite structure belongs to the *Pm*3*m* space group and is typified by strontium titanate (ST) with a unit-cell parameter $a = 3.905$ Å at room temperature.[1] When ST is cooled below $T_a \cong 108$ K, it undergoes a second-order improper ferroelastic phase transition[2] from cubic (*Pm*3*m*) to a centrosymmetric tetragonal (*I*4/*mcm*) phase[3–5] with a doubled primitive unit cell caused by antiphase rotations of the oxygen octahedra around one of the ⟨100⟩ axes.[2,6,7] The lowering of the symmetry at the phase transition was considered to be responsible for the appearance of several sharp lines in the Raman spectra of ST below T_a and a softening of two of these phonon frequencies as T_a is approached.[7] On the basis of these observations, Fleury, Scott, and Worlock[7] proposed that the soft mode at the Brillouin zone boundary (R point) is responsible for the improper ferroelastic transition in ST at T_a, with a frequency approaching zero as the temperature decreases to T_a. Fleury, Scott, and Worlock[7] also suggested that the doubling of the lattice constant at T_a leads to the folding of the Brillouin zone, so that the R point is in the zone center. Hence the number of zone-center excitations increases, and two new zone-center phonons, whose progenitor was the zone-boundary phonon, increase in frequency or harden as *T* is lowered below T_a.[7] This model was later confirmed by inelastic neutron-scattering measurements[2] and electron paramagnetic resonance (EPR) measurements[8–10] and was supported by an observed shift of the sound velocity at T_a.[11–13]

Along with spectroscopic techniques, such as Raman, the simplest method to investigate octahedral tilt transitions in perovskites is to observe the superlattice reflections, which appear upon cooling.[14] However, X-ray diffraction is largely insensitive to scattering from the oxygen sublattice, and therefore, it is difficult to detect the precise onset temperature of a structural phase transition by the appearance of superstructure reflections. Furthermore, the distortion of the cation sublattice is often quite small, and the associated peak splitting (if any) may be difficult to observe. Neutrons diffract strongly from oxygen, but even when available, extrapolation of the change in intensity of the superlattice reflections as a

* To whom correspondence should be addressed. Fax: +351-234-425300. E-mail: paula.vilarinho@ua.pt.
[†] University of Aveiro.
[‡] University of Sheffield.
[§] Czech Academy of Sciences.

(1) Mitsui, T.; Westphal, W. B. *Phys. Rev.* **1961**, *124*, 1354.
(2) Shirane, G.; Yamada, Y. *Phys. Rev.* **1969**, *177*, 858.
(3) Müller, K. A. *Phys. Rev. Lett.* **1959**, *2*, 341.
(4) Rimai, L.; deMars, G. A. *Phys. Rev.* **1962**, *127*, 702.
(5) Lytle, F. W. *J. Appl. Phys.* **1964**, *35*, 2212.
(6) Unoki, H.; Sakudo, T. *J. Phys. Soc. Jpn.* **1967**, *23*, 546.
(7) Fleury, P. A.; Scott, J. F.; Worlock, J. M. *Phys. Rev. Lett.* **1968**, *21*, 16.
(8) Müller, K. A.; Berlinger, W.; Waldner, F. *Phys. Rev. Lett.* **1968**, *21*, 814.
(9) Thomas, H.; Müller, K. A. *Phys. Rev. Lett.* **1968**, *21*, 1256.
(10) Müller, K. A.; Berlinger, W. *Phys. Rev. Lett.* **1971**, *26*, 13.
(11) Bell, R. O.; Rupprecht, G. *Phys. Rev.* **1963**, *129*, 90.
(12) Rupprecht, G.; Winter, W. H. *Phys. Rev.* **1967**, *155*, 1019.
(13) Fossheim, K.; Berre, B. *Phys. Rev. B: Condens. Matter Mater. Phys.* **1972**, *5*, 3292.
(14) Glazer, A. M. *Acta Crystallogr., Sect. B: Struct. Sci.* **1972**, *28*, 3384.

10.1021/cm071795c CCC: $37.00
Published on Web 12/04/2007

function of the temperature is required to pinpoint T_a. In situ electron diffraction (ED) is widely available, and electrons scatter from the oxygen sublattice with sufficient strength to form discrete reflections at $^1/_2\{ooo\}$ (where o = odd) positions below T_a. The major disadvantage is that the intensity of each reflection cannot be quantified; therefore, the amplitude of the tilt can only be qualitatively estimated. However, the presence or absence of weak superstructure reflections is unambiguous. Therefore, the onset temperature of the phase transitions and the nature of the tilting (antiphase or in-phase) can be identified.

Currently, there is significant interest in ST because of the repeated observation that dopants, such as Ca^{2+}, Mn^{2+}, and Bi^{3+}, on the Sr site induce a dielectric relaxation below room temperature[15–17] on the background of the incipient ferroelectric or quantum paraelectric behavior of undoped ST.[18] On the other hand, no polar anomaly was induced when La^{3+} was substituted on the Sr site nor when Mg^{2+} or Mn^{4+} were doped onto the Ti site.[19,20] However, if Mg^{2+} is substituted onto the Ti site as part of a complex solid solution, such as $SrTi_{1-y}(Mg_{1/3}Nb_{2/3})_yO_3$, a relaxation is observed.[21,22] Despite this considerable attention, the effect of dopants on T_a has largely been ignored. Two models for the effect of dopants on T_a are proposed in this work.

A. Octahedral Tilting and Tolerance Factor. Recently, Lemanov et al.[23] showed by acoustic methods that the onset of the improper ferroelastic phase transition for the solid solutions $Sr_{1-x}A_xTiO_3$ (where A = Ba, Pb, and Ca) correlates with the lattice parameter. The transition temperature T_a decreases with an increasing lattice parameter (Ba and Pb) and increases with a decreasing lattice parameter (Ca). On the other hand, for the composition $SrTi_{1-y}(Mg_{1/3}Nb_{2/3})_yO_3$, the transition temperature T_a increases together with the lattice parameter.[23] However, the apparent contradiction to this trend with $SrTi_{1-y}(Mg_{1/3}Nb_{2/3})_yO_3$ can be resolved by relating the change in T_a not to the lattice parameter but to the perovskite tolerance factor t[24]

$$t = \frac{r_A + r_O}{\sqrt{2}(r_B + r_O)} \quad (1)$$

where r_A and r_B are the average radii of ions occupying the A and B sites, respectively, and r_O is the ionic radius of the oxygen. Several authors have demonstrated that as t increases, T_a decreases and vice versa.[25,26] In the case of Ba (1.6 Å) or Pb (1.49 Å)[27] substitution onto the Sr (1.44 Å) site, r_A increases, leading to an increase in t, and therefore, T_a decreases. On the other hand, the t in the $SrTi_{1-y}(Mg_{1/3}Nb_{2/3})_yO_3$ system decreases because of an increase in the average r_B by substitution of Ti^{4+} (0.605 Å) ions by larger Mg^{2+} (0.72 Å) and Nb^{5+} (0.64 Å)[27] ions, which results in an increase of T_a similar to $Sr_{1-x}Ca_xTiO_3$.

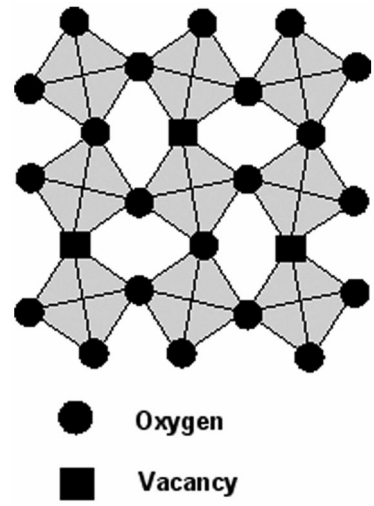

Figure 1. Schematic showing the cogwheel manner of octahedral rotations and a distribution of O vacancies.

B. Octahedral Tilting and Oxygen Vacancies. Substitution of Ti^{4+} ions with acceptor ions (e.g., Mg^{2+} on the Ti site) is known to induce oxygen vacancies ($V_O^{\bullet\bullet}$) according to the equation, in Kröger–Vink notation

$$Ti_{Ti} = Mg_{Ti}'' + V_O^{\bullet\bullet} \quad (2)$$

It is also well-documented that titanates can be reduced by sintering in low $P(O_2)$. The formation of Ti^{3+} ions is compensated by the formation of $V_O^{\bullet\bullet}$. The basis of tilting in perovskites is a cooperative long-range rotation of octahedra in a "cogwheel"manner as shown in Figure 1. Disruption of the connectivity within the octahedral layers by introducing $V_O^{\bullet\bullet}$ statistically decreases the correlation length of tilting/rotation. To compensate for this disruption, a greater driving force is required to induce a tilted structure, and therefore, T_a is suppressed. A decrease of T_a was found by neutron diffraction[28] and ultrasonic velocity measurements[29] in $SrTiO_3$ samples fired at low $P(O_2)$, presumably as a result of an increase in the concentration of $V_O^{\bullet\bullet}$.

In contrast, donor doping on, e.g., the A site with La^{3+}, is compensated ionically in two possible ways

$$Sr_{Sr} = La_{Sr}^{\bullet} + 1/4V_{Ti}'''' \quad (3)$$

$$Sr_{Sr} = La_{Sr}^{\bullet} + 1/2V_{Sr}'' \quad (4)$$

Compensation for $La_{Sr}^{\bullet}$ via V_{Ti}'''' and V_{Sr}'' does not induce $V_O^{\bullet\bullet}$ and will only affect the onset of tilting by considering

(15) Bednorz, J. G.; Müller, K. A. *Phys. Rev. Lett.* **1984**, *52*, 2289.
(16) Tkach, A.; Vilarinho, P. M.; Kholkin, A. L. *Appl. Phys. Lett.* **2005**, *86*, 172902.
(17) Ang, C.; Yu, Z.; Vilarinho, P. M.; Baptista, J. L. *Phys. Rev. B: Condens. Matter Mater. Phys.* **1998**, *57*, 7403.
(18) Müller, K. A.; Burkhard, H. *Phys. Rev. B: Condens. Matter Mater. Phys.* **1979**, *19*, 3593.
(19) Tkach, A.; Vilarinho, P. M.; Kholkin, A. L. *Ferroelectrics* **2004**, *304*, 917.
(20) Tkach, A.; Vilarinho, P. M.; Kholkin, A. L.; Pashkin, A.; Samoukhina, P.; Pokorny, J.; Veljko, S.; Petzelt, J. *J. Appl. Phys.* **2005**, *97*, 044104.
(21) Lemanov, V. V.; Sotnikov, A. V.; Smirnova, E. P.; Weihnacht, M. *Phys. Solid State* **2002**, *44*, 2039.
(22) Lemanov, V. V.; Smirnova, E. P.; Sotnikov, A. V.; Weihnacht, M. *Appl. Phys. Lett.* **2000**, *77*, 4205.
(23) Lemanov, V. V.; Smirnova, E. P.; Ukhin, E. V. *Phys. Solid State* **2004**, *46*, 1323 and references therein.
(24) Megaw, H. D. *Proc. Phys. Soc.* **1946**, *58*, 133.
(25) Woodward, P. M. *Acta Crystallogr., Sect. B: Struct. Sci.* **1997**, *53*, 32.
(26) Reaney, I. M.; Colla, E. L.; Setter, N. *Jpn. J. Appl. Phys.* **1994**, *33*, 3984.
(27) Shannon, R. D. *Acta Crystallogr., Sect. A: Found. Crystallogr.* **1976**, *32*, 751.
(28) Hastings, J. B.; Shapiro, S. M.; Frazer, B. C. *Phys. Rev. Lett.* **1978**, *40*, 237.
(29) Bauerle, D.; Rehwald, W. *Solid State Commun.* **1978**, *27*, 1343.

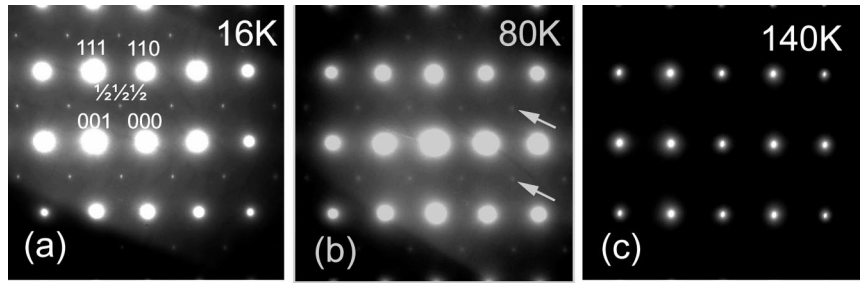

Figure 2. $\langle 110 \rangle_p$ zone axis electron diffraction patterns of undoped $SrTiO_3$ at (a) 16, (b) 80, and (c) 140 K.

how cation vacancies influence t. In ST, compensation for donor doping on the A site is generally considered to occur via V_{Sr}'', and therefore, t is further diminished and T_a is expected to increase. Moreover, the ionic radius of La^{3+} (1.36 Å) is smaller than that of Sr^{2+} (1.44 Å),[27] which should give an additional decrease in t and an increase in T_a.

The aim of this study is to assess the effect of dopants on T_a in ST using in situ Raman spectroscopy and ED to demonstrate the validity of the above models.

Experimental Section

$SrTiO_3$, $Sr_{0.975}Mn_{0.025}TiO_3$, $SrTi_{0.95}Mn_{0.05}O_3$, $Sr_{0.925}La_{0.05}TiO_3$, and $SrTi_{0.95}Mg_{0.05}O_{3-\delta}$ ceramics were prepared by a conventional mixed oxide method, in which the incorporation of dopant ions on the A or B site of the ST perovskite lattice was facilitated by the corresponding intentional deficit of the Sr or Ti precursor, as described in detail elsewhere.[30–32] In the case of Mn-doped ST systems, ceramics were batched assuming Mn^{4+} substitutes for Ti^{4+} and Mn^{2+} for Sr^{2+}. The presence of Mn^{2+} and Mn^{4+} on the A and B sites, respectively, in the appropriate ceramics sintered in air was confirmed by EPR experiments, the data from which are presented elsewhere.[33] In addition, $SrTi_{0.95}Mn_{0.05}O_3$ ceramics were sintered in O_2 and N_2 atmospheres.[32] Sintering in O_2 favors the formation of Mn^{4+}, whereas sintering in N_2 promotes $Mn^{2+/3+}$ on the B site, typically compensated by $V_O^{\bullet\bullet}$. The models for charge compensation in La- and Mg-doped ST have been presented above and are well-known.

ED patterns and micrographs were obtained using an in situ He cold stage (GATAN) on a Hitachi 9000 transmission electron microscopy (TEM) operated at 300 keV at temperatures ranging from 16 to 300 K. The local increase of temperature induced by the electron beam is difficult to quantify. In this experiment, parallel illumination conditions were used to obtain ED patterns, which minimize this effect. Even so, beam heating is estimated to be between 10 and 30 °C, depending upon the local microstructure of the thin foil. Sintered samples were prepared for TEM by grinding to a thickness of ~30 μm and ion beam milling using a BAL-TEC Ion Mill (RES 100).

Micro-Raman spectra were acquired in the back-scattering geometry using a Renishaw Raman microscope after the ceramics were excited by the argon laser beam, with the wavelength of 514.5 nm and the spot size of 1–2 μm in diameter. The measurements were performed at fixed temperatures from 10 to 300 K.

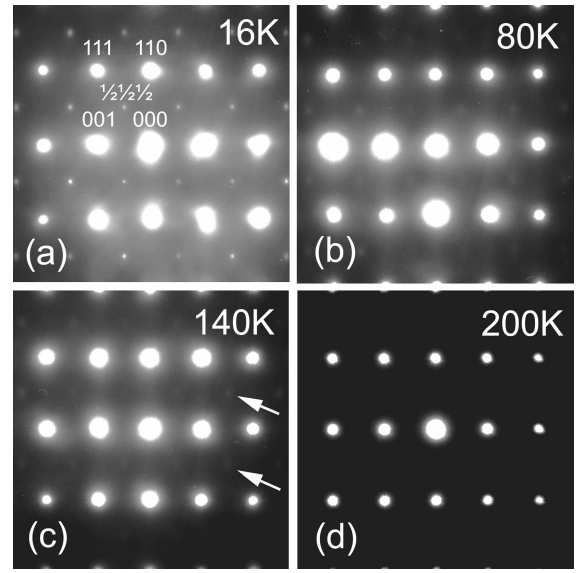

Figure 3. $\langle 110 \rangle_p$ zone axis electron diffraction patterns of $Sr_{0.975}Mn_{0.025}TiO_3$ at (a) 16, (b) 80, (c) 140, and (d) 200 K.

Results and Discussion

A. In Situ ED. Figure 2 shows zone axis electron diffraction patterns (ZADPs) obtained at 16, 80, and 140 K with the electron beam parallel to a $\langle 110 \rangle$ pseudocubic direction for undoped ST. The $^1/_2\{ooo\}$ superlattice reflections, related to the tilting of oxygen octahedra in the antiphase and marked in the diffracted images, appeared upon cooling below 100 K, consistent with T_a (108 K) reported in the literature. Figure 3 shows the $\langle 110 \rangle_p$ ED patterns obtained for $Sr_{0.975}Mn_{0.025}TiO_3$ and recorded at 16, 80, 140, and 200 K, and room temperature. The $^1/_2\{ooo\}$ superlattice reflections were detected up to ~140 K. For $SrTi_{0.95}Mn_{0.05}O_3$ sintered in air, $^1/_2\{ooo\}$ superlattice reflections are more diffuse than those of undoped ST and could only be detected up to ~80 K, as shown in Figure 4. It was concluded therefore that T_a is suppressed by Mn^{4+} substitution for Ti^{4+} on the B site but enhanced by Mn^{2+} substitution for Sr^{2+} on the A site. For Mn^{2+} on the Sr site, the increase in T_a is attributed to a decrease in t because Mn^{2+} (~1.27 Å) has a considerably smaller ionic radius than Sr^{2+} (1.44 Å).[27] Conversely, Mn^{4+} (0.53 Å) is smaller than Ti^{4+} (0.605 Å),[27] and substitution results in an increase in t, suppressing T_a. The valence of Mn is difficult to control in perovskite-structured ceramics. However, in previous work,[30] it has been

(30) Tkach, A.; Vilarinho, P. M.; Kholkin, A. L. *Appl. Phys. A: Mater. Sci. Process.* **2004**, *79*, 2013.
(31) Tkach, A.; Vilarinho, P. M.; Kholkin, A. L. *Acta Mater.* **2005**, *53*, 5061.
(32) Tkach, A.; Vilarinho, P. M.; Kholkin, A. L. *Acta Mater.* **2006**, *54*, 5385.
(33) Laguta, V. V.; Kondakova, I. V.; Bykov, I. P.; Glinchuk, M. D.; Tkach, A.; Vilarinho, P. M. *Phys. Rev. B: Condens. Matter Mater. Phys.* **2007**, *76*, 054104.

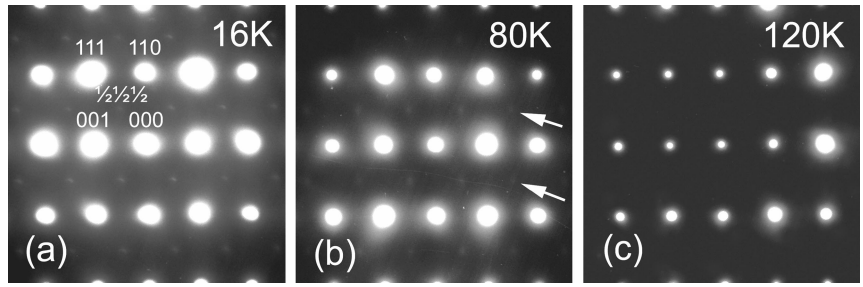

Figure 4. $\langle 110 \rangle_p$ zone axis electron diffraction patterns of $SrTi_{0.95}Mn_{0.05}O_3$ ceramics at (a) 16, (b) 80, and (c) 120 K.

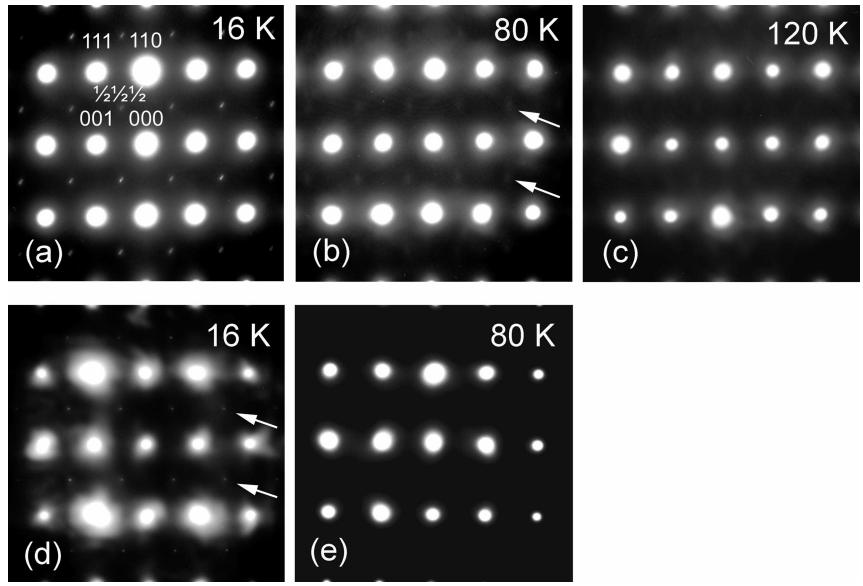

Figure 5. $\langle 110 \rangle_p$ zone axis electron diffraction patterns obtained at 16 (a and d), 80 (b and e), and 120 K (c) from the grains of $SrTi_{0.95}Mn_{0.05}O_3$ ceramics sintered in oxygen (a, b, and c) and nitrogen (d and e) atmospheres.

shown that the lattice parameter of $SrTi_{1-y}Mn_yO_3$ decreases linearly in accordance with Vegard's law as y increases from 0 to 0.15 with $da/dy \approx 0.1$ Å. Mn^{3+} (0.58/0.645 Å low/high spin) and Mn^{2+} (0.67/0.83 Å low/high spin) are both larger than Mn^{4+} and would increase the lattice parameter with an increasing concentration. Moreover, EPR data have shown that Mn^{4+} and Mn^{2+} are the major substituent ion on the appropriate sites.[33]

Experiments were also performed on $SrTi_{0.95}Mn_{0.05}O_{3-\delta}$ ceramics sintered in O_2 and N_2 atmospheres. In principle, sintering in O_2 promotes Mn^{4+}, whereas in N_2, Mn^{2+} and Mn^{3+} form, typically compensated by $V_O^{\bullet\bullet}$. Figure 5 shows $\langle 110 \rangle_p$ ZADPs taken at different temperatures from the grains of $SrTi_{0.95}Mn_{0.05}O_{3-\delta}$ ceramics, sintered in O_2 (parts a–c of Figure 5) and N_2 (parts d and e in Figure 5). In addition to the basic reflections of the cubic perovskite, superlattice reflections appear for O_2-sintered $SrTi_{0.95}Mn_{0.05}O_{3-\delta}$ at ~80 K, almost at the same temperature as for samples sintered in air. This confirms that Mn^{4+} is present not only in O_2-sintered but also as the major dopant ion in air-sintered $SrTi_{0.95}Mn_{0.05}O_{3-\delta}$ ceramics. On the other hand, for samples sintered in N_2, superlattice reflections were not observed at 80 K and were only present at 16 K, implying that T_a is suppressed, presumably because of the formation of $V_O^{\bullet\bullet}$. To further verify the effect of $V_O^{\bullet\bullet}$ on T_a, Mg ions were substituted onto the B site. Mg ions have a stable 2+ valence state, and charge compensation is well-documented to occur via $V_O^{\bullet\bullet}$,

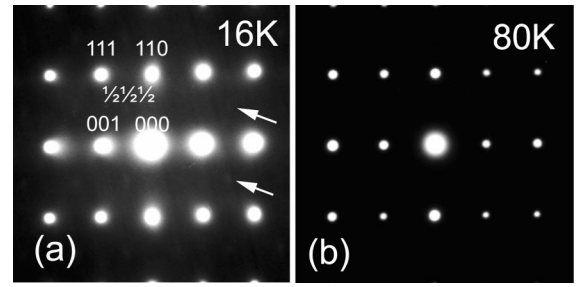

Figure 6. $\langle 110 \rangle_p$ zone axis electron diffraction patterns of $SrTi_{0.95}Mg_{0.05}O_{3-\delta}$ at (a) 16 and (b) 80 K.

according to eq 2. Figure 6 shows the $\langle 110 \rangle_p$ zone axis electron diffraction patterns for $SrTi_{0.95}Mg_{0.05}O_{3-\delta}$, recorded at 16 and 80 K. No superlattice reflections are observed at 80 K, but weak spots appear at $^1/_2\{ooo\}$ positions at ~16 K, confirming that the acceptor doping the B site in ST suppresses T_a despite an apparent decrease in t when the larger Mg^{2+} ion substitutes for Ti^{4+}.

Figure 7 presents $\langle 110 \rangle_p$ ED patterns from $Sr_{0.925}La_{0.05}TiO_3$, recorded at 16 K and room temperature. Superlattice reflections associated with antiphase rotation of the oxygen octahedra at the $^1/_2\{ooo\}$ positions are evident in each image. T_a has therefore increased to above room temperature as t decreases because of the substitution of the smaller La^{3+} (1.36 Å) ion on the Sr site. In addition, the formation of

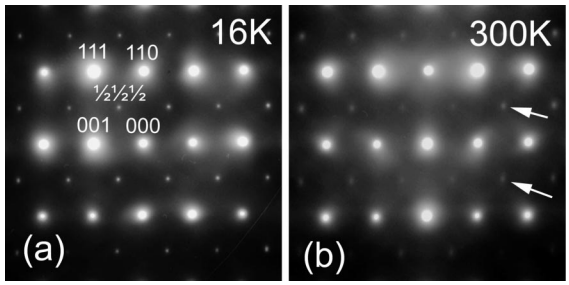

Figure 7. $\langle 110 \rangle_p$ zone axis electron diffraction patterns from grains of $Sr_{0.925}La_{0.05}TiO_3$ ceramics at (a) 16 and (b) 300 K.

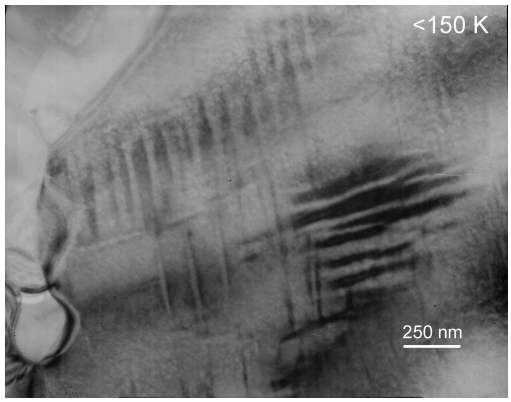

Figure 8. Bright-field image of ferroelastic domains, observed in $Sr_{0.925}La_{0.05}TiO_3$ ceramics below 150 K.

V_{Sr}'' to compensate for the charge because of donor doping further reduces t, favoring an increase in T_a.

Although, the $^1/_2\{ooo\}$ superlattice reflections are present at room temperature, their intensities increase strongly upon cooling, qualitatively consistent with an increase in amplitude of rotation and indicative of a second-order phase transition. At ~150 K, ferroelastic domains form within the sample, as illustrated in Figure 8. Upon cooling, as the amplitude of tilt increases, the spontaneous strain also increases. Eventually, dependent upon the local elastic boundary criteria, anisotropic strain in the grains is relieved by the formation of a domain structure. The temperature interval (150 K) between the onset of cell doubling and the formation of domains is consistent with the occurrence of an improper ferroelastic phase transition in which the amplitude of rotation is the order parameter rather than spontaneous strain, i.e., spontaneous strain results from the octahedral rotation. The above results are summarized in Table 1.

B. Raman Spectroscopy. Micro-Raman spectra of $Sr_{0.975}Mn_{0.025}TiO_3$, $SrTi_{0.95}Mn_{0.05}O_3$, $Sr_{0.925}La_{0.05}TiO_3$, and $SrTi_{0.95}Mg_{0.05}O_{3-\delta}$ ceramic samples sintered in air are shown in Figure 9 for selected temperatures. As known from the literature[34] and observed for our ceramics, the spectra of undoped ST (not shown) are characterized by dominant second-order features at room temperature, whereas the first-order IR-active transverse optical and longitudinal optical modes as well as two R modes are seen below 110 K, consistent with our ED data (Figure 2). Spectra of $Sr_{0.975}Mn_{0.025}TiO_3$ ceramics are similar to those of undoped ST, but there is one difference pointing to the incorporation of Mn into ST lattice. The modes (at 147 and 450 cm^{-1}, marked by arrows in Figure 9) from the R point of the Brillouin zone, which become permitted Γ-point modes decrease below T_a, are of higher intensity below 110 K. Moreover, for $Sr_{0.975}Mn_{0.025}TiO_3$, the R modes can be seen well in Figure 9a up to 130 K, transforming into shoulders at 140 K and disappearing upon further heating to 150 K. Such behavior indicates that, in $Sr_{0.975}Mn_{0.025}TiO_3$ ceramics, the lattice dynamics is affected by dopant ions and T_a is increased, as evidenced by the ED patterns in Figure 3.

On the other hand, the Raman spectra of $SrTi_{0.95}Mn_{0.05}O_3$, shown in Figure 9b, are very different from those of undoped ST.[34] In addition, the R modes are hardly detectable above 70 K, implying that T_a has been suppressed; an observation entirely consistent with the ED data presented in Figure 4 for $SrTi_{0.95}Mn_{0.05}O_3$. The transformation of the spectra and decrease of T_a are also indicative for the introduction of Mn into ST lattice but at the other site, confirming that the obtained ceramics are in agreement with the batched stoichiometry.

The spectra of $Sr_{0.925}La_{0.05}TiO_3$ ceramics, presented in Figure 9c, reveal R modes up to 180 K, pointing to an increase in T_a. Above this temperature, no mode could be detected at 450 cm^{-1}, whereas the mode at 147 cm^{-1} seems to be overlapped by an adjacent one. Therefore, in contrast to $Sr_{0.975}Mn_{0.025}TiO_3$, the Raman spectra of $Sr_{0.925}La_{0.05}TiO_3$, where R modes are absent above 180 K, are in some contradiction to the ED patterns with superlattice reflections observed at room temperature (Figure 7). This may be explained by some degree of chemical inhomogeneity in the ceramic. Despite this discrepancy, it is evident that the general trend of La^{3+} substitution for Sr^{2+} increasing T_a is confirmed.

In the spectra for $SrTi_{0.95}Mg_{0.05}O_{3-\delta}$ (Figure 9d), the R modes are detected only below 30 K, consistent with the in situ ED data (Figure 6), for which superstructure reflections were observed at 16 K. It is concluded therefore that Mg^{2+} substitution for Ti^{4+} strongly suppresses T_a because of the formation of $V_O^{\bullet\bullet}$. Table 1 summarizes the Raman as well as ED data obtained from the above samples. In addition, Figure 10 represents the transition temperature T_a as a function of the tolerance factor t for ST-based materials with A- and B-site substitutions, as reported by Lemanov and co-authors,[21,35] Ranjan et al.,[36] and in this work. The tolerance factor was calculated using ionic radii by Shannon.[27] It is evident from the Figure 10 that T_a is correlated to t and that the relationship between the tolerance factor and the improper ferroelastic phase transition temperature is linear. Even in the case of La^{3+} substituting for Sr^{2+}, where the size of strontium vacancy is not known and the tolerance factor was calculated assuming the vacancy size to be the same as that of the Sr^{2+} ion, no great deviation was observed. The only point that falls out of

(34) Petzelt, J.; Ostapchuk, T.; Gregora, I.; Rychetský, I.; Hoffmann-Eifert, S.; Pronin, A. V.; Yuzyuk, Y.; Gorshunov, B. P.; Kamba, S.; Bovtun, V.; Pokorný, J.; Savinov, M.; Porokhonskyy, V.; Rafaja, D.; Vaněk, P.; Almeida, A.; Chaves, M. R.; Volkov, A. A.; Dressel, M.; Waser, R. *Phys. Rev. B: Condens. Matter Mater. Phys.* **2001**, *64*, 184111.

(35) Smirnova, E. P.; Sotnikov, A. V.; Kunze, R.; Weihnacht, M.; Kvyatkovskii, O. E.; Lemanov, V. V. *Solid State Commun.* **2005**, *133*, 421.

(36) Ranjan, R.; Pandey, D.; Lalla, N. P. *Phys. Rev. Lett.* **2000**, *84*, 3726.

Table 1. Features of Undoped and Doped ST in Light of R Modes in Raman Spectra and Superlattice Reflections in TEM–ED Patterns

compositions	ionic radii[a] (Å)	R modes in Raman spectra	superlattice reflections in TEM–ED patterns	T_a
$SrTiO_3$	$r_{Sr^{2+}}{}_{12} = 1.44$, $r_{Ti^{4+}}{}_{6} = 0.605$	detected up to 110 K	bright at 16 and 80 K, not detected at 140 K	110 K, in accordance with the literature
$Sr_{0.975}Mn_{0.025}TiO_3$	$r_{Mn^{2+}}{}_{12} = 1.27$	detected up to 140 K	bright at 16 and 80 K, weak at 140 K, not detected at 200 K	≥140 K
$SrTi_{0.95}Mn_{0.05}O_3$	$r_{Mn^{4+}}{}_{6} = 0.53$	detected up to 70 K	bright at 16 K, weak at 80 K, not detected at 120 K	≤80 K
$Sr_{0.925}La_{0.05}TiO_3$	$r_{La^{3+}}{}_{12} = 1.36$	detected up to 180 K	bright up to 300 K	≥180 K, locally up to room temperature
$SrTi_{0.95}Mg_{0.05}O_{3-\delta}$	$r_{Mg^{2+}}{}_{6} = 0.72$	detected up to 20 K	weak at 16 K, not detected at 80 K	≤30 K

[a] Valence and coordination number of ions are indicated as super- and subscripts, respectively.

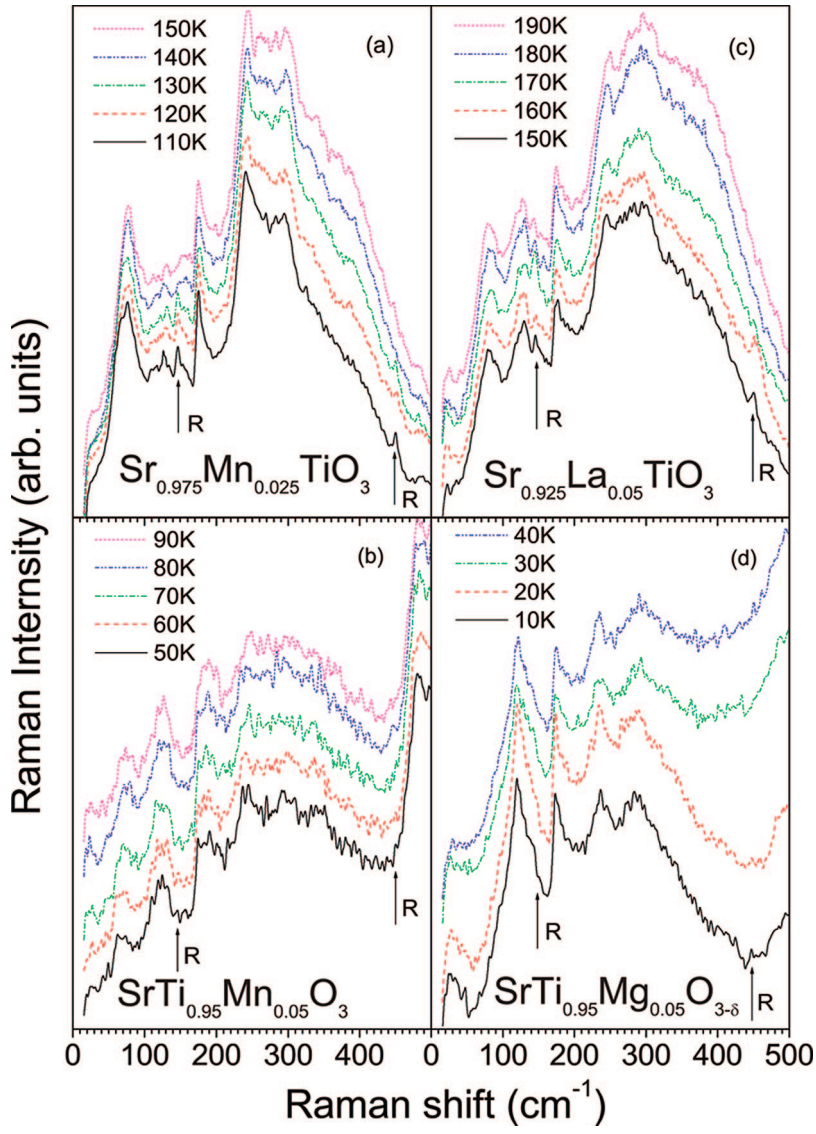

Figure 9. Raman spectra of $Sr_{0.975}Mn_{0.025}TiO_3$ (a), $SrTi_{0.95}Mn_{0.05}O_3$ (b), $Sr_{0.925}La_{0.05}TiO_3$ (c), and $SrTi_{0.95}Mg_{0.05}O_{3-\delta}$ (d) ceramics at selected temperatures, with an indication of the approximate position of R modes.

this trend is Mg^{2+} substituting for Ti^{4+}. In this case, the suppression of T_a by the formation of $V_O^{\bullet\bullet}$ is stronger than the effect associated with the tolerance factor. This suggests that disruption of the interconnectivity of the O octahedral network has the greatest influence on T_a. However, upon inspection, a simple linear relationship between $[V_O^{\bullet\bullet}]$ and T_a is unlikely. It is more likely that, at a certain $[V_O^{\bullet\bullet}]$, coupling of O rotations becomes statistically improbable and that, as this percolation limit is approached, T_a is catastrophically suppressed.

Conclusions

For doped ST ceramics, qualitative lattice vibrational and structural analyses have shown that (i) R modes in Raman spectra and $^1/_2\{ooo\}$ superlattice reflections in ED patterns

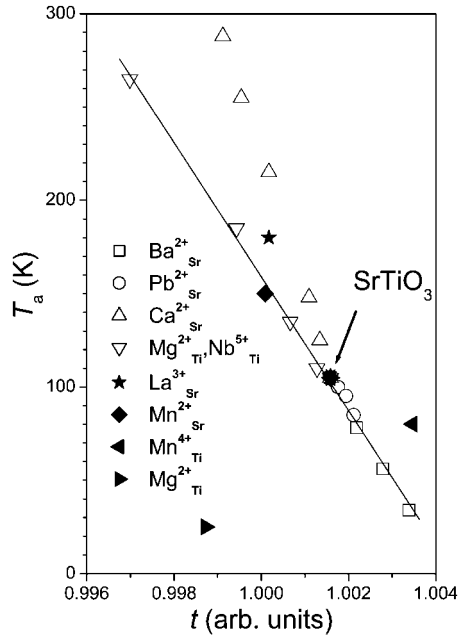

Figure 10. Improper ferroelastic phase transition temperature T_a for ST-based materials with Sr^{2+} substituted by Ba^{2+}, Pb^{2+}, Ca^{2+}, Mn^{2+}, and La^{3+} and Ti^{4+} substituted by Mn^{4+}, Mg^{2+}, and $Mg^{2+}_{1/3}Nb^{5+}_{2/3}$ as a function of the tolerance factor *t*. Several data points are included for some substituents because *t* varies with the dopant concentration. Data points marked by solid symbols correspond to our own work; open symbols are taken from refs 21, 35, and 36.

of $Sr_{0.975}Mn_{0.025}TiO_3$ are observable at ~140 K, at least 30 K higher than that of undoped ST, (ii) T_a in $SrTi_{0.95}Mn_{0.05}O_3$ sintered in air or O_2 is ~80 K, at least 30 K lower than that of undoped ST, (iii) $^1/_2\{ooo\}$ superlattice reflections in ED patterns of $SrTi_{0.95}Mn_{0.05}O_{3-\delta}$ sintered in N_2 are observable far below 80 K, (iv) T_a is decreased to <30 K with respect to undoped ST for $SrTi_{0.95}Mg_{0.05}O_{3-\delta}$, and (v) La^{3+} substituted on the Sr site increases T_a to >180 K and allows for the formation of ferroelastic domains upon cooling below 150 K.

From these data, it can be unambiguously concluded that, as *t* increases, e.g., samples for which Mn^{4+} substitutes for Ti^{4+}, T_a is suppressed. Furthermore, as *t* decreases, e.g., for formulations with Mn^{2+} and La^{3+} on the A site, T_a increases. For acceptor doping in which $V_O^{\bullet\bullet}$ are formed, e.g., with Mg^{2+} or $Mn^{3+/2+}$ on the B site, T_a decreases because of the formation of $V_O^{\bullet\bullet}$. Therefore, all data are entirely consistent with the models proposed.

Although this is a fundamental study on a classic electroceramic, $SrTiO_3$, there are broader technological ramifications to this work. It is now paramount to consider the effect that not only dopants in functional ceramics have on, e.g., T_c, but also on T_a. As an example, Zheng et al.[37] demonstrated the effect of increasing T_a on piezoelectric properties in their study of Sr-doped PZT. Increasing T_a to above room temperature resulted in a reduction in d_{33} from 640 pC/N (12 mol % SrO) to 250 pC/N (16 mol % SrO) because of the suppression of the domain wall motion and a commensurate decrease in the extrinsic contribution to piezoelectric properties.

Acknowledgment. The authors acknowledge FCT, FEDER, and FAME Network, under contract FP6-500159-1.

CM071795C

(37) Zheng, H.; Reaney, I. M.; Lee, W. E.; Jones, N.; Thomas, H. *J. Am. Ceram. Soc.* **2002**, *85*, 2337.